Indonesian Journal of Earth Sciences, Vol. 2, No. 2 (2022): 203-225

P-ISSN: 2798-1134 | E-ISSN: 2797-3549 | DOI: 10.52562/injoes.v2i2.409

Indonesian Journal of Earth Sciences

http://journal.moripublishing.com/index.php/injoes

Relationship of the Seasonal Vegetation Indices against the NDVI and LST in the Region of Kamuku Game Reserve and Kwiambana National Park, Nigeria

AbdulAzeez Onotu Aliyu, Terwase Tosin Youngu, Adamu Bala, Samuel Azua, Swafiyudeen Bawa, Muhammad Kabir Agboola

Department of Geomatics, Ahmadu Bello University, Zaria, Kaduna State, Nigeria

Correspondence: abdulonotu@gmail.com

Received: 24 September 2022; Accepted: 13 November 2022; Published: 26 December 2022

Abstract: While it is anticipated that there would be some similarities amongst spectral Vegetation Indices (VIs) because the majority of the indices use the red and NIR bands, it is also expected that there would be some variances. The NDVI, derived earlier by Rouse (1973), and is the commonly used VI, there have meagre understanding of the relationship between the NDVI and another VIs. Similarly, investigations on the correlation between LST and other VIs (other than NDVI) in both dry and raining seasons have not been adequately explored. This motivated the study to determine the seasonal correlation of some spectral VIs against the NDVI and LST over the forest reserve area. The study investigated two categories of VIs: slope-based and distance-based. It derived spectral VIs from Landsat 8 images for dry (January) and raining (August) seasons; and estimated LST from MODIS. The findings showed that the ARVI, GNDVI and TVI not only showed resemblance in appearance with the NDVI in both seasons, but also had a high coefficient of correlation: ARVI = 0.973, 0.964; GNDVI = 0.919, 0.879; TVI = 0.779, 0.716. Based on this finding, the ARVI, GNDVI and TVI can be used to supplant the NDVI for biomass related studies in the study area. The study further revealed that the LST-VIs relationship was negative for both dry and rainy seasons, except for the distance-based VIs (DVI, SAVI, MSAVI) that specifically had a positive correlation with the LST. The LST was strongly correlated with the GNDVI, TVI, NDVI, ARVI ($0.664 \geq r \geq 0.598$). However, the strength of the correlation for the LST-VIs in the raining season was very weak ($0.003 \leq r \leq 0.245$). The study concluded that the correlation of the LST versus the ARVI, GNDVI, NDVI, and TVI can be used for climate related studies.

Keywords: Correlation, dry and rainy seasons, forest reserve, LST, NDVI, vegetation indices

INTRODUCTION

As the major producer in ecosystems, vegetation plays an essential role in earth systems and global change science (She et al., 2015). Vegetation is a term generally for a region's plant life; it refers to plant-provided soil cover and is the most ubiquitous biotic element in the biosphere (Chu, 2019). Some vegetation is permanent, i.e. it lasts or stands for months or years, such as forest reserves; others, such as seasonal crops, are only cultivated for a few months at a time (Chandra, 2011). In remote sensing, the reflectance of vegetation in the electromagnetic spectrum (spectral reflectance or emission characteristics of vegetation) is governed by the chemical and morphological properties of the organs or leaves on the surface (Zhang & Kovacs, 2012). The theory behind this is the significant absorption of green healthy vegetation in the red channel owing to leaf pigments such as chlorophyll and strong reflection of vegetation in the Near Infrared (NIR) channel of the electromagnetic spectrum due to interior leaf structure. Healthy vegetation, on the

other hand, reflects more in the red wavelength than diseased or sparse vegetation. Barren terrain and soil reflect moderately in both the red and NIR spectrums (Holme et al., 1987).

Vegetation can efficaciously impact Land Surface Temperature (LST) by selectively absorbing and reflecting solar radiation energy and regulating latent and sensible heat exchange (Yuan et al., 2017). Areas where vegetation is high, like in central Africa, tend to retain LST due to high absorption (due to low albedo) and storage of solar energy by plants throughout the day. In the Sahara Desert, where vegetation is limited, absorption is lower (due to high albedo) and the LST varies considerably (Preveldello et al., 2019) from one location to another. LST is a critical parameter in studying surface matter exchange, surface energy balance, and surface physical and chemical processes, and it is now widely utilized in soil studies, hydrology, biology, geochemistry, and other fields (Tomlinson et al., 2011; Hao et al., 2016), which is important to the study of environmental change (Deng et al., 2018). LST can be defined as the skin temperature of the surface, which refers to soil surface temperature for bare soil, canopy surface temperature of vegetation for densely vegetated ground (Khandelwal et al., 2017). LST measures the ground temperature of the earth surface. LST can be thought of as what one would feel when one places his hand on the ground at a particular location. LST on the contrary, is not air temperature.

Importantly, spectral vegetation indices (VIs) are important algorithms for the extraction of information of vegetation condition (Salas & Henebry, 2014). Zhou et al. (2014) stated that various vegetation indices derived from remotely sensed satellite data have been developed and are widely utilized for assessing changes in the physiological state and biophysical characteristics of plants (She et al., 2015). The basic purpose of VIs is to extract as much information as possible from spectral reflectance data by removing variability caused by vegetation features (e.g. LAI, vegetation cover) and to reduce the effects of soil, atmospheric, and sun-target-sensor geometry (Moulin, 1999). VIs are related to vegetation type (trees, bushes, grass, etc.); precisely, type of leaves, their shape, inclination angle; crop architecture; plant growth stage (senescence); leaf pigment content: chlorophyll and other pigments like carotene, xanthophyll etc. (their composition and distribution in leaves); and water content of plants, and many other (Jensen, 2007; Liang, 2005; Purkis & Klemas, 2011, Yengoh et al., 2015).

Although a significant number of spectral VIs have been proposed, yet the Normalized Difference Vegetation Index (NDVI), introduced by Rouse (1974) is the most well-known and frequently utilized in remote sensing applications linked to various researches such as: global vegetation studies (Huete et al., 1997; Zhang et al., 2016); agricultural crop growth and yield prediction (Panda et al., 2010; Lopresti et al., 2015); land degradation (Xu et al., 2009; Higginbottom & Symeonakis, 2014).

While it is anticipated that there would be some similarities amongst VIs due to the fact that the bulk of the indices utilize the NIR band, it is also expected that there will be some variances (Vogelmann, 1990). The NDVI, derived earlier by Rouse (1973), and is the commonly used VI. There are rarely studies that compared the NDVI with other VIs. Rather, what is available in literature is the relationship between NDVI with some sort of climatic or biophysical variables such as Leaf Area Index (LAI), which can be found in Wang & Huang (2010); precipitation in Wang et al., (2020); temperature in Sun & Kafatos, (2007); evapotranspiration in Xiong & Qiu, (2011); and albedo in Kafer et al., (2020). Similarly, Lawrence & Ripple (1998) carried out a study on correlation of vegetation cover with some vegetation indices (NDVI, SAVI, OSAVI, MSAVI, Green Vegetation Index). Again, Panek et al. (2020) evaluated within-field relationships between satellite-derived VIs Vegetation indices [Normalized Difference Vegetation Index (NDVI), Soil-Adjusted Vegetation Index (SAVI), modified SAVI (mSAVI), modified SAVI 2 (mSAVI2), Infrared Percentage Vegetation Index (IPVI), Global Environmental Monitoring Index (GEMI), and Ratio Vegetation Index (RVI)] and grain yield (winter wheat and triticale).

Previous studies on the correlation between LST and NDVI were primarily concerned with examining the influence of urbanization on anomalous heat (Urban Heat Island) in cities. Some of these studies can be found in Deng et al. (2018), Guechi et al. (2021), and Koko et al. (2021). Furthermore, Macarof et al. (2018) investigated the correlation between LST and NDVI, MSAVI,

and EVI only in the warmth season. Similarly, Alademomi et al. (2020) assessed the association of LST, NDVI and EVI with land cover changes in dry season. These studies used the simple linear regression analysis to determine the relationship between LST and the studied VIs. Although, Tariq et al. (2020) studied the relationship between LST and land cover indices: NDVI, Normalized Difference Water Index (NDWI), Normalized Difference Surface Index (NDSI), Normalized Difference Built-up Index (NDBI), and Built-up Index (BI), yet studies on the relationship between LST and other VIs (apart from NDVI, MSAVI, EVI) in both dry and rainy seasons have not been sufficiently addressed or reported.

Thus, there is meagre information on the relationships between VIs against the NDVI and VIs against the LST in forested areas at different atmospheric conditions (weather). Also, little is known as to which VI is suitable for the study area. As a result, this study aimed at assessing seasonal relationship between certain satellite-derived spectral VIs against the NDVI and LST over the forest reserve in parts of Kamuku game reserve and Kwianbana national park of Birnin Gwari and Maru Local Government Areas of Kaduna and Zamfara states, Nigeria. The rationale for this study was to evaluate the performance of the VIs against the NDVI and LST based on the vegetation condition, and to ascertain the most appropriate vegetation index for the study area.

The scope of the study was to derive VIs for the dry and rainy seasons; computing LST for dry and rainy seasons; and evaluating the relationships between the VIs with the NDVI and LST as reference variables. The study is descriptive and explorative. The study area was chosen because of its dense vegetation and being part of Nigeria's forest reserves. The derived spectral VIs are: (1) Slope-based indices: the Normalized Difference Vegetation Index (NDVI), Enhanced Vegetation Index (EVI), Green Vegetation Index or Green Normalized Vegetation Index (GNDVI), Transformed Vegetation Index (TVI), and Atmospherically Resistant Vegetation Index (ARVI), Normalized Difference Greenness Index (NDGI). (2) Distance-based indices: Distance Vegetation Index (DVI), Soil Adjusted Vegetation Index (SAVI), and Modified Soil Adjusted Vegetation Index (MSAVI). However, this study did not consider other distance-based VIs such as: Perpendicular Vegetation Index (PVI) and Transformed Soil Adjusted Vegetation Index (TSAVI) that make use of soil line parameters (slope and intercept), which can be got from two-dimensional graph (or bi-spectral plot) of NIR versus red (Silleos et al., 2006).

STUDY AREA

The study area is a forest reserve that is part of the Kamuku game reserve and the Kwianbana national park. It is located within Longitude 6° 8' 8.65" E and 6° 38' 24.42" E of the Central Meridian, and Latitude 10° 39' 55.02" N and 11° 16' 15.84" N of the Equator as shown in Figure 1. It has a land area of 271,584.763 hectares. The Kamuku Park is located in the Birnin Gwari Local Government Area, which is located west of Kaduna State, and is near to the Kwiambana Game Reserve to the north-east. Kwiambana Game Reserve is located in Maru Local Government Area, Zamfara state. Both Kaduna and Zamfara states are located in north-west geopolitical zone of Nigeria. Kamuku was established in 1936 as the Native Authority Forest Reserve of Birnin Gwari under the then Northern Nigeria Government (Kamuku National Park, 2022), whereas Kwiambana was submitted to the United Nations Educational, Scientific, and Cultural Organization (UNESCO) in November 1995 as a potential World Heritage Center (UNESCO, 2022). The study area is densely forested trees and shrubs. It experiences two seasons: dry season (November to April) and raining season (May to October). Its minimum and maximum altitudes are 407 and 409 metres above mean sea level, respectively. The study area has served as shelter for bandits currently scourging, especially northern region of the country.

METHODS

This section describes the datasets used, techniques used for the data processing and analysis are summarized in the workflow diagram in Figure 2.

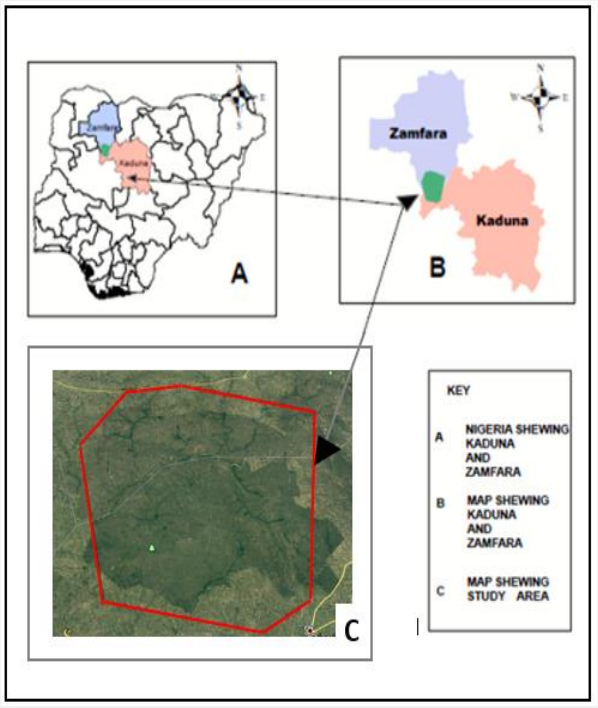

Figure 1. Inset map of the study area.

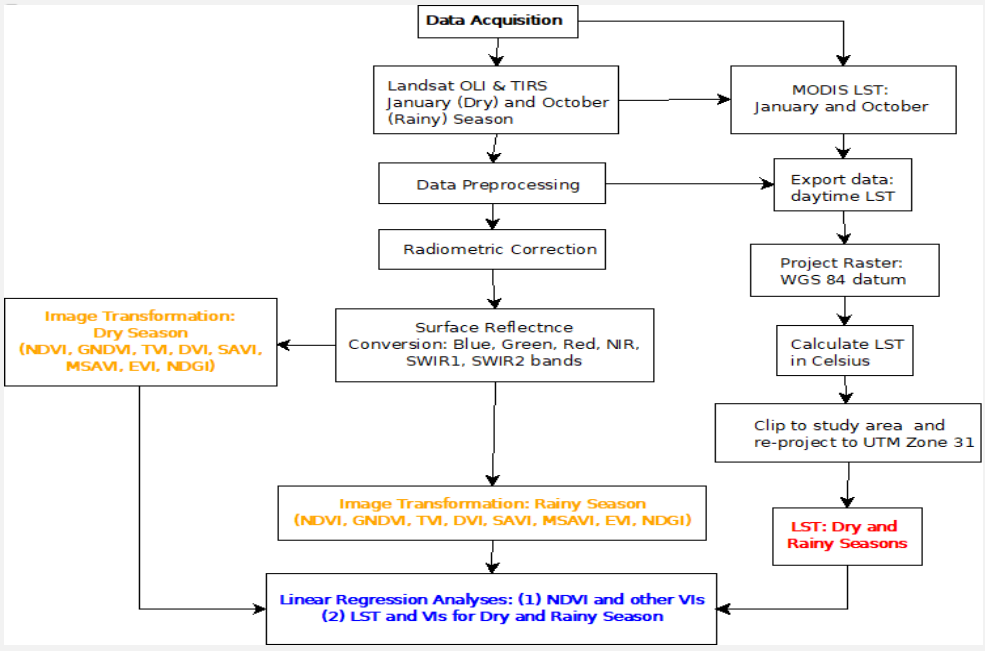

Figure 2. Workflow diagram of the study.

Datasets and source

The VIs were derived using Landsat OLI and TIRS data from 2018, which were obtained from the United States Geological Survey (USGS) website (http://www.earthexplorer). The attributes of the datasets are listed in Table 1. Landsat 8 images were obtained during the dry season in January (2018) and the rainy season in October (2018). The Landsat 8 bands came in a Digital Number (DN) scale, the bands that were used are: band 2 (blue), band 3 (green), band 4 (red),

band 5 (NIR), band 6 (SWIR 1), and band 7 (SWIR 2), in that order. The LST was retrieved from the Moderate Imaging Spectrometer (MODIS) LST and emissivity 8-day version 6 level 3 data in sinusoidal projection format. MODIS LST data includes both LST and emissivity. The MOD11A2 is composite of the Terra (day) and Aqua (night) LSTs and is in Kelvin. It was obtained from the website of the National Aeronautics and Space Administration (NASA) (http://www.earthdata.org) (See Table 1). Figure 2 depicts the method for retrieving the LST.

Table 1. Attributes of the datasets used

S/N	Data Type	Year	Cell Size	Path/Row	Purpose	Source
1	Landsat 8	07 Jan., 2018	30m	190/52	Indices derivation	USGS
2	Landsat 8	22 Oct., 2018	30m	190/52	Indices derivation	USGS
3	MOD11A2	01 Jan., 2018 09 Jan., 2018 17 Jan., 2018	1000m	h18: v7	LST retrieval	NASA
4	MOD11A2	08 Oct., 2018 16 Oct., 2018 24 Oct., 2018	1000m	h18: v7	LST retrieval	NASA

Radiometric Correction

From Figure 2, each Landsat image was radiometrically calibrated, which entails going from DN to Top-of-Atmosphere (TOA) radiance, and then to surface reflectance. The surface reflectance measurement is essential because the majority of indices use it as input, and because surface reflectance more accurately portrays the difference in land covers than other remotely sensed image measures (digital number and radiance). The radiometric calibration takes into account the following factors: earth-sun distance or geometry; atmospheric scattering and absorption; band width (the spectrum at which radiation is received); and sun illumination at the time of acquisition. The algorithms for the radiometric corrections are shown in equations 1, 2 and 3.

1. Conversion of DN to radiance (for TM and ETM+)

$$L_\lambda = \frac{(LMAX\lambda - LMIN\lambda)}{(Qcalmax - Qcalmin)}(Q_{CAL} - Q_{CALMIN}) + L_{MIN\lambda} \quad (1)$$

2. Conversion of DN to TOA Radiance (for OLI and TIRS)

$$L_\lambda = M_L \times Q_{cal} + A_L \quad (2)$$

3. Conversion of TOA radiance to TOA reflectance

$$\rho\lambda = \frac{\pi \times L_\lambda \times d_2}{ESUN_\lambda \times COS\theta_{sz}} \quad (3)$$

Where:
L_λ = spectral radiance at the sensor's aperture; Q_{CAL} = Quantized calibrated pixel value (DN);
Qcalmin = Maximum quantized pixel value (corresponding to $LMAX_\lambda$) in DN = 255;
$LMIN_\lambda$ = spectral radiance that is scaled to Q_{CAL} max (W. m-1. ster-1. µm-1);
$LMAX_\lambda$ = Spectral radiance that is scale to Q_{CAL} min (W. m-1. ster-1. µm-1);
M_L = Band-specific multiplicative rescaling factor from the metadata (RADIANCE_MULT_BAND_x, where x is the band number).
A_L = Band-specific additive rescaling factor from the metadata (RADIANCE_MULT_BAND_x, where x is the band number);
$\rho\lambda$ = unitless TOA or planetary reflectance;
$L\lambda$ = spectral radiance at the sensor's aperture;

d = Earth-Sun distance in astronomical units from nautical handbook or interpolated values from Julian day calendar and day of the year (DOY) in excel file;
ESUNλ = mean solar exoatmospheric spectral irradiance. To be found in Landsat 5 handbook;
COSSZ = solar zenith angle in degrees. (SZ = 90º - ΘSE), where SE = sun elevation [(Chander & Markham, 2003), (Lathrop, 2004), (Yale, 2013)].
The radiometric corrections were carried out using the Fast Line Atmospheric Analysis of Spectral Hypercube (FLAASH) tool in ENVI v5.2.

Thereafter, to convert the images to surface reflectance, the Dark Object Subtraction (DOS) method, which is an atmospheric correction technique was applied to the TOA reflectance in equation (3). The basic premise of this approach is that certain pixels in the Landsat image are dark or completely in shadow (which are not intended to reflect radiation), and their outgoing radiances (known as path radiance) are sensed at the sensor owing to atmospheric scattering (Chavez, 1988; Amidon, 2014; O'neil-Dunne, 2014; Gilmore et al., 2015; GSP, 2019). As a result, the darkest pixel (with the lowest radiance value) was subtracted from each pixel value. ENVI v5.2 and ArcGIS v10.5 were used for the radiometric corrections.

$$\text{Surface Reflectance} = \rho\lambda - \rho_{Dark\ Object} \quad (4)$$

Where $\rho_{Dark\ Object}$ is the darkest pixel in the image and the least reflectance value.

Derivation of VIs for dry and wet seasons

Having calibrated the Landsat bands to reflectance scale, the VIs were then computed using the Raster Calculator tool in ArcMap v10.5 by applying their respective mathematical expressions. This is shown in Table 2.

Table 2. Mathematical expressions for VIs and their sources

No	Expression	Reference
1	$DVI = NIR - RED$	Richardson & Wiegand (1977), Tucker (1979)
2	$NDVI = \frac{NIR - RED}{NIR + RED}$	Rouse et al. (1973), Carlson et al. (1997)
3	$TVI = \sqrt{NDVI + 0.5}$	Rouse (1974), Deering et al. (1975)
4	$GVI\ or\ GNDVI = \frac{NIR - GREEN}{NIR + GREEN}$	Gitelson et al. (1996), Panda et al. (2010)
5	$NDGI = \frac{GREEN - RED}{GREEN + RED}$	Baret & Guyot (1991), Gitelson et al. (2002)
6	$SAVI = \frac{NIR - RED}{NIR + RED + L} * (1 + L)$	Huete (1988), Haboudane et al. (2004)
7	$ARVI = \frac{[NIR - (2RED - BLUE)]}{[NIR + (2RED - BLUE)]}$	Kaufman & Tanre (1992) Pinty & Verstraete (1992) Falk et al. (2004)
8	$EVI = \frac{NIR - RED}{NIR + C1 * RED - C2 * BLUE + L}(1 + L)$	Gao et al. (2000) Huete et al. (2002)

No	Expression	Reference
9	$MSAVI = \frac{2\mathrm{NIR} + 1 - \sqrt{(2NIR = 1)^2 - 8(\mathrm{NIR} - \mathrm{R})}}{2}$	Qi et al. (1994)

[1]*L = soil brightness correction factor (taken as 0.5).*
[2]*C1, C2 = coefficients of aerosol resistance term (C1 = 6.0, C2 = 7.5)* (Huete et al., 2002).

The feature space of NIR and red bands represented on a scatter plot for dry season is shown in Figure 3.

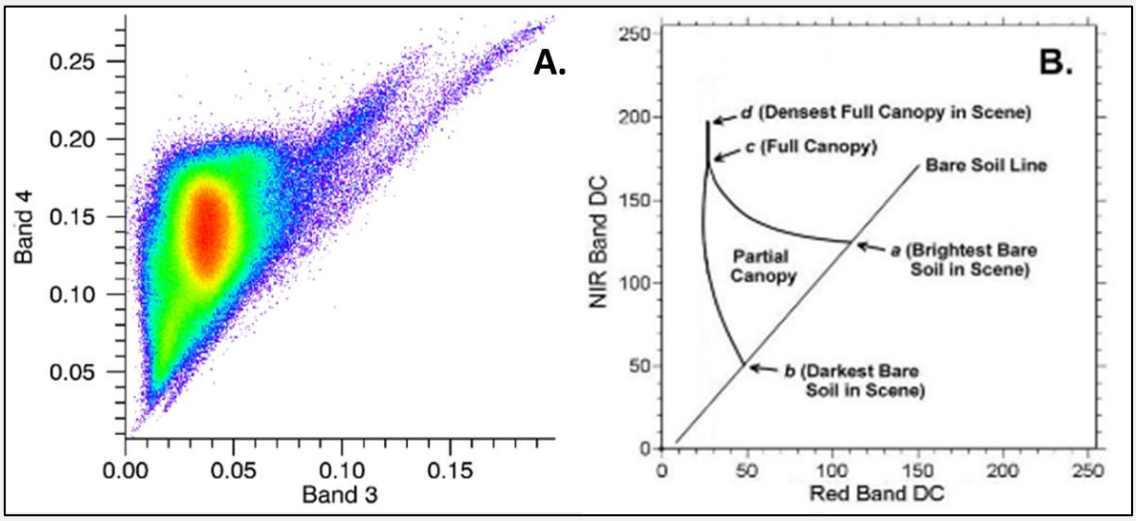

Figure 3. (a) NIR-RED scatter plot of pixel values of dry season image (Authors' Lab work); (b) Schematic diagram of the features of the scatter plot (after Maas & Rajan, 2010).

From Figure 3, the diagonal of the triangle in the scatter plot is termed as a soil line (Baig et al., 2014). The center of the plot, which is in red color represents a partial canopy (Maas & Rajan, 2010) or sparse vegetation (Njomo, 2008). The region of the dense green vegetation implies that the NDVI has a great pixel value, because of high abundance of chlorophyll leadig to a low reflectance in the red channel together with plentiful stacking of leaves (Njomo, 2008).

Land Surface Temperature Retrieval

The decision to retrieve LST from MODIS was made because the MOD11A2 version 6 data has improvements over version 2 and 3 in that cloud contaminated values have been removed, the Look-up table (LUT) for the split-window LST retrieval algorithm has been updated, and the classification of emissivity values (bare soil/rocks) has been adjusted (Wan, 2013). Figure 2 depicts the method for retrieving LSTs. Because the MOD11A2 data is a composite of day and night LST, the daytime component was used and exported as a separate data set. The study employed daytime LST because vegetation has a stronger cooling effect on LST during the day than at night (Sun & Kafatos, 2007). The exported LST file originally in sinusoidal projection, which is a pseudo-cylindrical equal area projection that depicts the complete parallels of the Earth's surface as straight lines that are uniformly spaced and at their real distances (LP DAAC, 2017). This was projected to the Geographic Coordinate System (GCS) 1984 datum of the World Geodetic System (WGS). Then, as stated in equation 5, it was scaled with a scale factor of 0.02 (LP DAAC, 2017) and converted to degrees Celsius.

$$\text{LST °C} = (\text{MODIS data} \times 0.02) - 273.15 \quad (5)$$

As a result, the LST was then clipped to the study area and re-projected to WGS 1984 datum, UTM zone 31. This was required to ensure an overlay with the Landsat 8 derivatives and the extraction of their values into sample points.

Relationship between NDVI against other VIs and LST against the VIs

The relationship between the NDVI and other VIs, as well as the LST and other VIs, was determined using simple linear regression analysis. The NDVI was considered as the dependent variable in the first linear regression analysis, whereas the other VIs were treated as independent variables. Subsequently, the LST was designated as the dependent variable and the VIs as the independent variables. To accomplish this, the derived VIs from Landsat 8 in 30m cell size and the retrieved LSTs from MODIS in 1000m cell size were resampled to 1000m such that the centroid of the cells of the indices coincided with the centroid of the LSTs. This also allowed for the creation of sample points that were common to both datasets. A systematic simple random sampling technique was used to generate sample points having a dimension of 2000m-by-2000m. This was accomplished by using fishnet tool in ArcGIS v10.5 to create rectangular cells that perfectly suit the study area. The fishnet tool generated 668 sample points based on a 2000m-by-2000m dimension as shown in Figure 4. The pixel values of each VI and LST were then extracted onto the 668 sample points using "extract values to points" tool in ArcMap v10.5. Thus, the simple linear regression analysis was carried out in Microsoft Excel utilizing the XLSAT add-in. The coefficient of determination (R^2) and the coefficient of correlation (r) were calculated. As a result, the coefficient of correlation was used to make conclusions and generalizations.

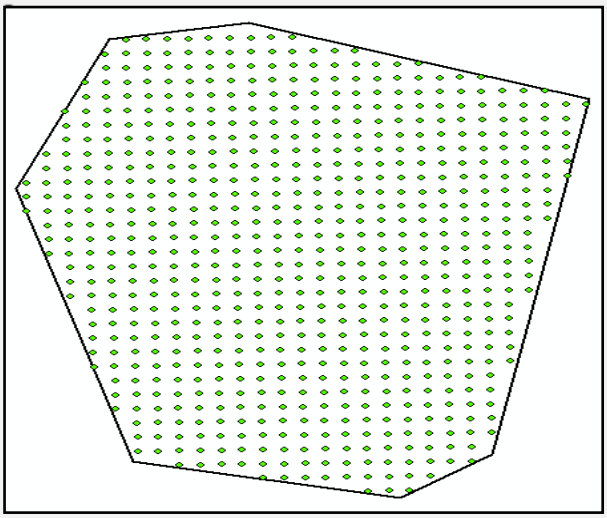

Figure 4. Generated systematic random sample points.

RESULTS AND DISCUSSION

Derived Vegetation Indices in Dry and Rainy Seasons

Descriptive statistics

The VIs are described using descriptive statistics (minimum, maximum, mean, standard deviation, and coefficient of variation, CV). The CV is used to illustrate how the VIs spread or dispersed throughout the study area. CV < 1 denotes low spread, whereas CV >= 1 denotes high spread. The spread of the VIs in dry season is ranked as follows: ARVI > NDGI > MSAVI > EVI > SAVI > NDVI > GNDVI > TVI respectively as shown in Table 3. Similarly, the spread of the VIs in raining season is ranked as follows: NDGI > DVI > MSAVI > ARVI > EVI > SAVI/NDVI > GNDVI

> TVI respectively. The VIs have a low spread in both the dry and raining seasons, but only the NDGI has a large spread (CV >= 1) in the raining season, as shown by the spike in Figure 5. Furthermore, in both seasons, the NDGI and MSAVI have a wider distribution than other VIs. As demonstrated in Figure 5, the VIs in dry season have a larger dispersion than the VIs in raining season in the study area.

Table 3. Simple statistics of VIs for both dry and rainy season

S/N	VI	Dry Season (January)					Rainy Season (October)				
		Min	Max	Mean	SD	CV	Min	Max	Mean	SD	CV
1	DVI	-0.06	0.21	0.09	0.03	0.33	-0.08	0.42	0.15	0.03	0.2
2	NDVI	-1	1	0.49	0.12	0.24	-1	0.94	0.70	0.09	0.13
3	TVI	0.13	1.22	0.99	0.06	0.06	0.01	1.20	1.09	0.04	0.04
4	GNDVI	-1	0.91	0.60	0.08	0.13	-1	0.91	0.72	0.07	0.1
5	NDGI	-0.36	1	0.17	0.06	0.35	-0.39	0.29	0.05	0.05	1
6	SAVI	-0.15	0.42	0.20	0.05	0.25	-0.21	0.65	0.32	0.04	0.13
7	ARVI	-1	1.82	0.33	0.16	0.48	-1	0.95	0.63	0.11	0.17
8	EVI	-0.13	0.42	0.19	0.05	0.26	-0.17	0.75	0.32	0.05	0.16
9	MSAVI	-0.11	0.39	0.17	0.05	0.29	-0.15	0.71	0.27	0.05	0.19

NOTE: *Coefficient of Variation:* $CV = \frac{SD}{Mean}$. *CV < 1 = low dispersion or variance. CV ≥ 1 = high dispersion. SD = Standard Deviation.*

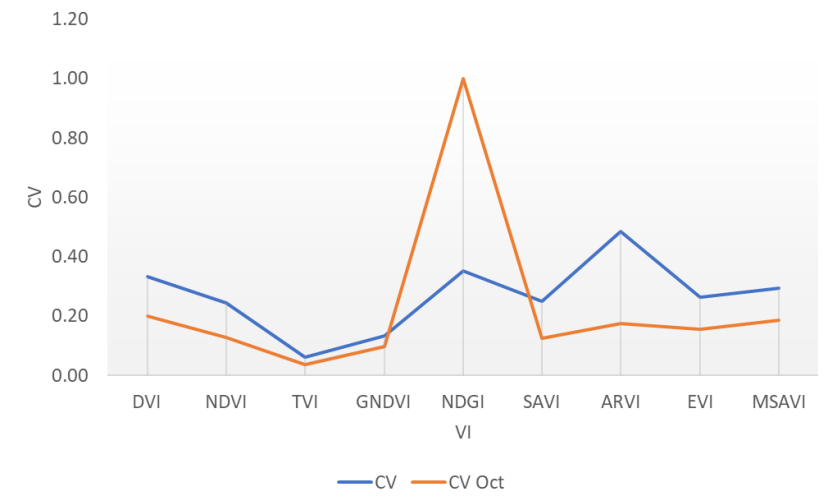

Figure 5. A plot of CV of the VIs for dry and rainy season

Visual inspection

The derived VIs both in dry and raining seasons are shown in Figures 6 and 7. Vegetation is represented in green color while bare ground is shown in deep purple color. Areas with minimal vegetation are shown in light purple color (Figures 6 and 7). By visual inspection, bare ground can be observed to be exposed along the margins of the four cardinal points (N, S, E, W) in the ARVI, NDGI, NDVI, and TVI for the dry season (Figure 6). However, bare ground was seldom exposed inside the study area for the DVI, EVI, GNDVI, MSAVI, and SAVI. The DVI, SAVI, and MSAVI are most suited for usage in dry regions with sparse vegetation and pixels that include a combination of green plant and soil background (Silleos et al., 2006). The NDGI (Figure 6f) revealed more bare ground than other VIs in the dry season. In this study, the VIs in dry season showed low vitality in

vegetation, as it was in the month of January when rainfall had ceased. Similarly, the VIs of the raining season showed strong vitality in plants, as it occurred in August when rainfall is usually at its peak in the study area. The aforestated is in conformity with the weather conditions of the study area. Furthermore, for the VIs in raining season, bare ground can be found to be exposed within the study area as revealed by DVI, EVI, MSAVI, NDGI, and SAVI (Figure 7b, c, e, f, h).

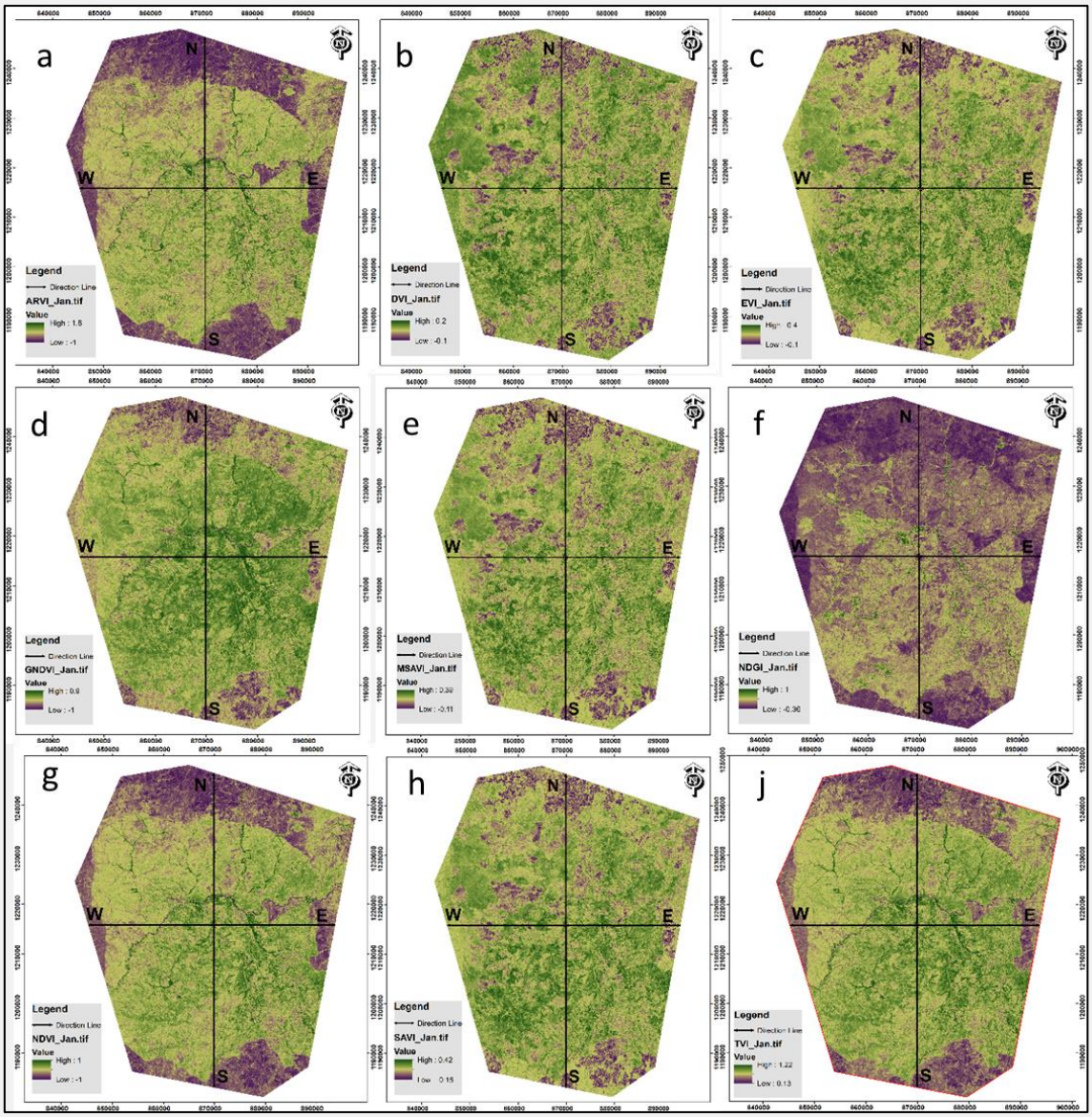

Figure 6. Derived Spectral VIs for dry season. (a) ARVI; (b) DVI; (c) EVI; (d); GNDVI; (e) MSAVI; (f) NDGI; (g) NDVI; (h); SAVI; (i) TVI.

This is in contrast to the notion that the study area should be lush with greenery in the raining season, where flora thrives. This can be based on the fact that the DVI, SAVI and MSAVI are distance-based VIs (they cancel out the influence of soil brightness when vegetation is sparse and pixels include a mixture of green vegetation and soil backdrop). For the EVI and NDGI, the study made no deduction on the reason. On the other hand, ARVI, GNDVI, NDVI, and TVI indicated the greenness of vegetation in raining season.

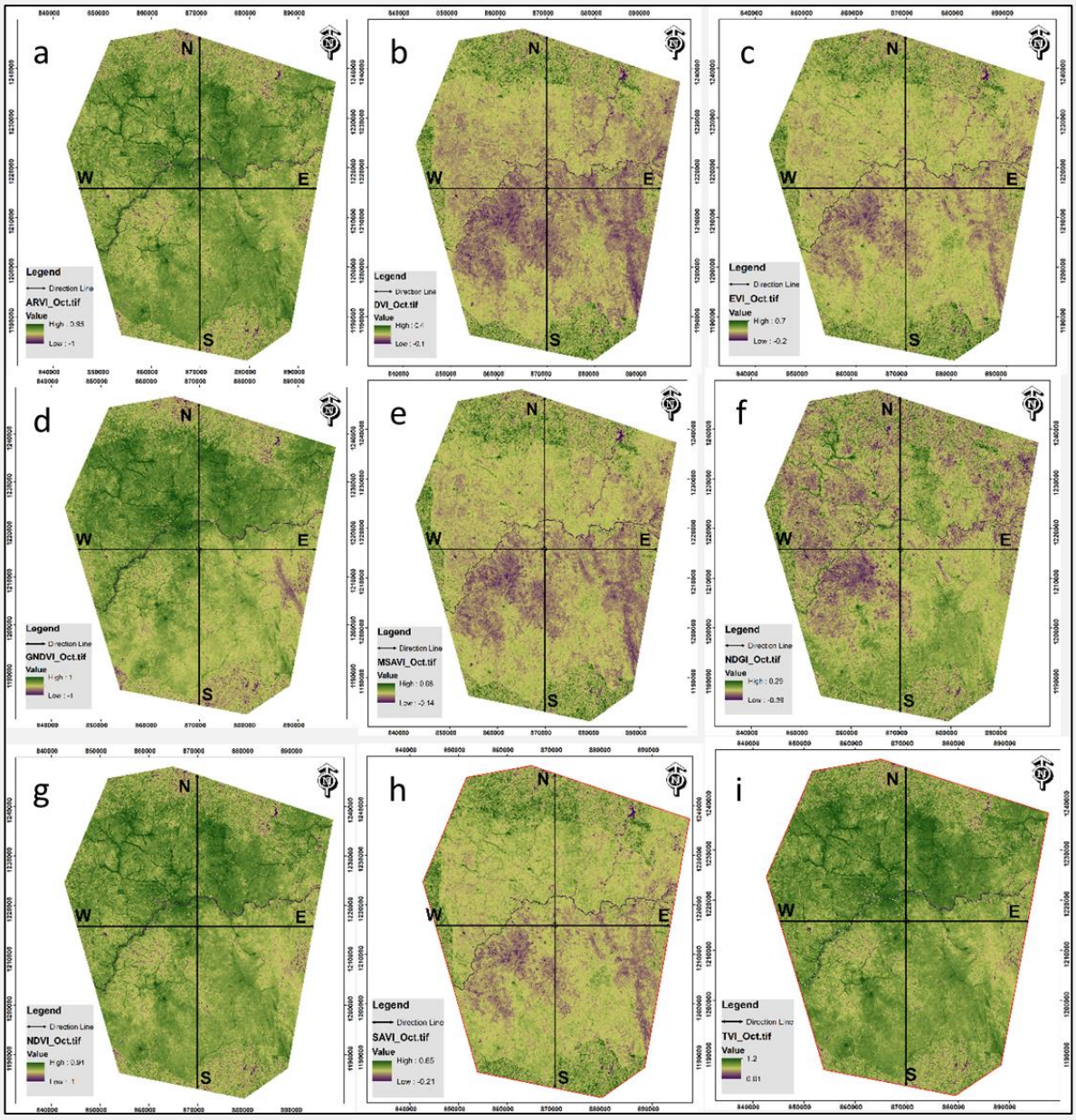

Figure 7. Derived Spectral VIs for raining season. (a) ARVI; (b) DVI; (c) EVI; (d) GNDVI; (e) MSAVI; (f) NDGI; (g) NDVI; (h) SAVI; (i) TVI.

The NDVI, being the earlier derived VI by Rouse (1973), is the renowned VI and commonly used in the geospatial scientific community for vegetation related studies. In this study, the ARVI, GNDVI and TVI show resemblance in appearance with the NDVI in both dry and raining season. Therefore, it is suggested that the ARVI, GNDVI and TVI can be used to supplant the NDVI for vegetation related studies in the study area.

Retrieved LST of Dry and Raining Seasons

Figure 8 depicts the retrieved LST for both the dry and rainy seasons (a and b). The minimum and maximum LSTs of dry season were 30.53°C and 36.93°C respectively, while the minimum and maximum LSTs of wet season are 28.58°C and 34.09°C. High LST is shown in red, while low LST is shown in blue. High LST can be noticed near the southern axis of the study area throughout both seasons (Figure 7). According to the NDVI, ARVI, NDGI, EVI, and TVI, the region with high LST corresponds to exposed bare ground (which has low heat absorption) (Figure 6). In both seasons,

high LST can be found in the northern axis; high LST can also be found in the western and eastern axes; and low LST can be found in the middle of the four cardinal points of the study area. It is obvious from the LST values that LST rises during the dry season and falls during the wet season. Low LST values corresponded to vegetation-rich locations in both the dry and wet seasons. The next section examines the degree of the correlation between the LST and the derived VIs.

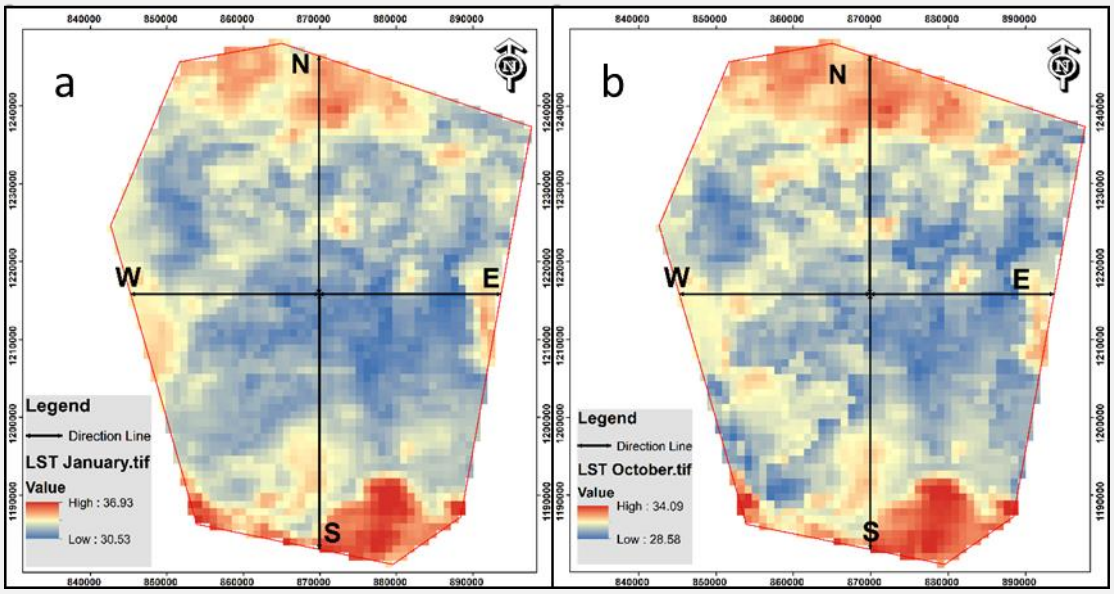

Figure 8. Retrieved LST. (a) Dry season. (b) Rainy season

Relationship between NDVI and other VIs in Dry and Rainy Seasons

Because of the fact that majority of the indices utilize the NIR and red bands, it is expected that there would be some similarities among the VIs on one hand and variances on the other hand. This necessitated their comparison. The scatterplots in Figures 9 and 10 show the correlation analysis of the relationship between NDVI and other derived VIs for dry and wet seasons, as does the correlation of coefficients in Table 4. The relationship between NDVI and the VIs are discussed in two folds: direction and strength of the correlation. The Scatterplots explain the direction of the correlation. The scatterplots of NDVI (dependent variable) *vs* VIs (independent variables) show that in both rainy seasons, the NDVI exhibited a positive linear correlation with the DVI, TVI, GNDVI, NDGI, SAVI, ARVI, EVI, and MSAVI (Table 4). This meant that in both the rainy seasons, the greater the NDVI, the higher the index. The reason for the positive correlation between the NDVI and the VIs is because the mathematical representation of the VIs comprises either an NIR or a red band, which is common to all the VIs. Interestingly, the DVI, SAVI, and MSAVI, which are distance-based vegetation indices (they cancel out the influence of soil brightness when vegetation is sparse and pixels include a mixture of green vegetation and soil backdrop), exhibit a positive correlation with the NDVI as well. Because the NDVI has a positive correlation with individual VIs, scatterplots of NDVI *vs* individual VIs revealed no surprising patterns.

Table 4 shows the correlation of coefficient of the NDVI *vs* the VIs in the dry season in terms of the intensity of the correlation. According to Cohen *et al.* (2013), the linear regression coefficient is determined using the correlation coefficient (r), with 0.31-0.5 representing a weak correlation, 0.51-0.7 representing a normal correlation, 0.71- 0.90 representing a strong correlation, and 0.91-1.0 representing a very strong correlation.

Importantly, all of the correlations between the NDVI and the VIs were statistically and highly significant (p-values < 0.01). The ARVI exhibited the most positive correlation with the NDVI ($r=0.973$), followed by the GNDVI, which also had a significant positive correlation with the NDVI ($r=0.919$). NDVI performed well with the TVI ($r=0.779$), NDGI ($r=0.754$), and EVI

(0.707), all of which had a positive strong correlation. Furthermore, NDVI (r=0.511), MSAVI (r=0.612), and SAVI (r=0.681) demonstrated a normal positive correlation. The distance-based VIs displayed a normal correlation with the NDVI, but the slope-based VIs had significant and very strong relationships with the NDVI in the dry season.

Table 4. Linear regression between NDVI and other VIs

S/N	Dry Season		Rainy Season	
	Linear Regression	r	Linear Regression	r
1	NDVI = 2.323 DVI + 0.262	0.561	NDVI = 1.820 DVI + 0.422	0.530
2	NDVI = 1.301 TVI – 0.803	0.779	NDVI = 1.351 TVI – 0.291	0.716
3	NDVI = 1.436 GNDVI – 0.387	0.919	NDVI = 1.301 GNDVI – 0.247	0.879
4	NDVI = 1.493 NDGI + 0.735	0.754	NDVI = 0.955 NDGI + 0.752	0.612
5	NDVI = 1.620 SAVI + 0.156	0.681	NDVI = 1.230 SAVI + 0.309	0.635
6	NDVI = 0.766 ARVI+0.2343	0.973	NDVI = 0.797ARVI – 0.196	0.964
7	NDVI = 1.710 EVI + 0.164	0.707	NDVI = 1.083 EVI + 0.359	0.604
8	NDVI = 1.595 MSAVI + 0.215	0.612	NDVI = 1.043 MSAVI + 0.408	0.567

NOTE: Generated at Confidence Interval of 99% (p-values < 0.01). r = coefficient of correlation. Sample points = 668.

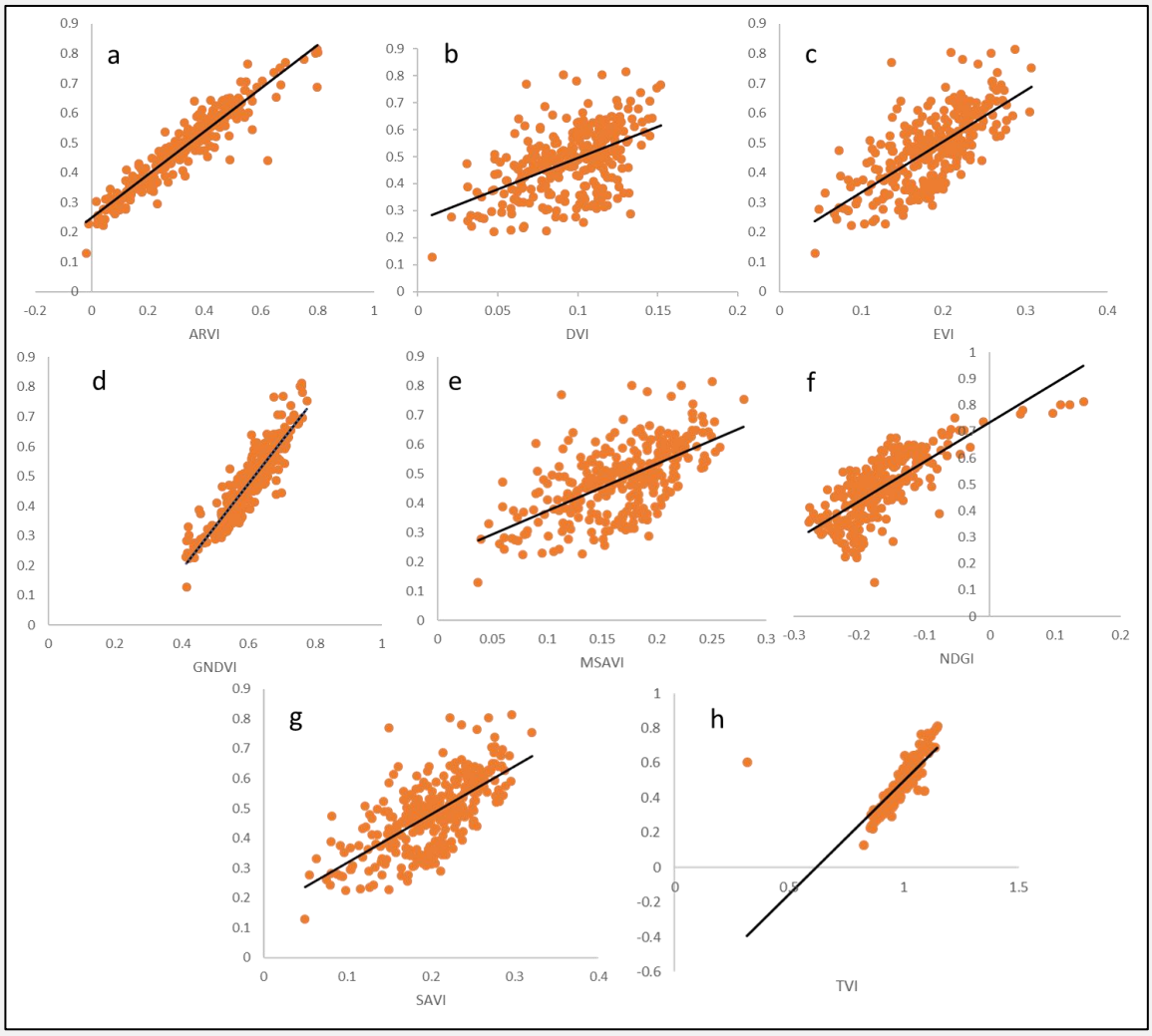

Figure 9. Scatterplots of NDVI versus VIs for dry season. (a) ARVI; (b) DVI; (c) EVI; (d) GNDVI; (e) MSAVI; (f) NDGI; (g) SAVI; (h) TVI.

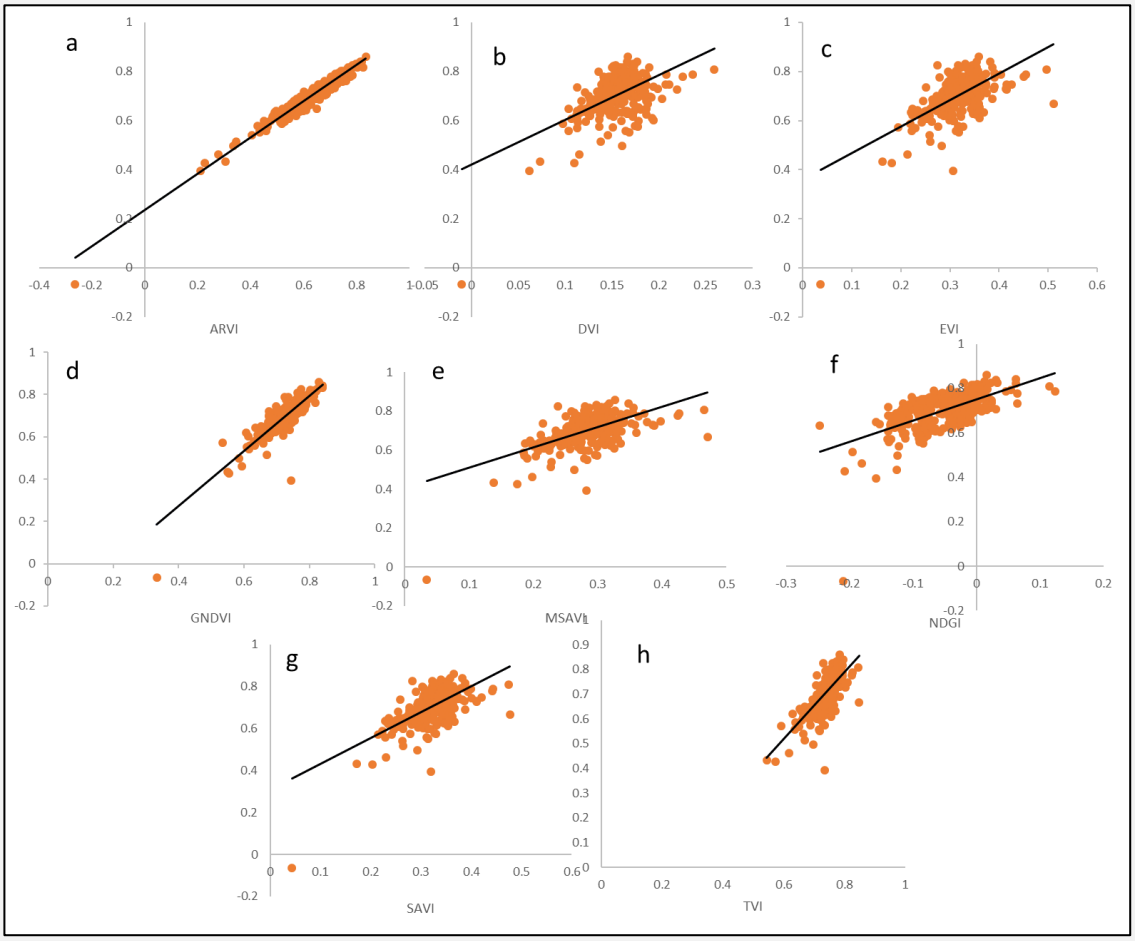

Figure 10. Scatterplots of NDVI versus VIs for rainy season. (a) ARVI; (b) DVI; (c) EVI; (d) GNDVI; (e) MSAVI; (f) NDGI; (g) SAVI (h) TVI.

Consequently, during the rainy season, ARVI fared best with the NDVI with a "r" value of 0.964. TVI (r=0.716) and GNDVI (r=0.879) performed better with the NDVI, both had a substantial positive correlation. The DVI (r=0.549), MSAVI (r=0.567), EVI (r=0.604), NDGI (r=0.612), and SAVI (r=0.635) all demonstrated a normal correlation with the NDVI. Similarly, in the rainy season, the distance-based VIs (DVI, MSAVI) exhibited a normal correlation with the NDVI, with the exception of SAVI, which had a strong correlation. Meanwhile, the slope-based VIs continue to have a strong correlation with the NDVI during the rainy season.

In general, the correlation between the VIs and the NDVI was positive in both the dry and rainy seasons. The VIs in the dry season demonstrated a larger positive correlation with the NDVI than the VIs in the rainy season. Importantly, the ARVI, GNDVI, and TVI are highly correlated with the NDVI and they also show resemblance in appearance with the NDVI in both seasons. However, lack of similar study on the correlation of the NDVI and other VIs in literature, the study did not cross-reference the results of the correlation of NDVI against other VIs with related studies.

Relationship between LST and the VIs in dry and rainy seasons

The scatterplots in Figures 11 and 12 show the relationship between LST and the computed VIs for dry and raining seasons, as does the correlation of coefficients in Table 5. The scatterplots of LST (dependent variable) vs VIs (independent variables) for the dry season indicated that the LST had a negative correlation with all the VIs: ARVI, DVI, EVI, GNDVI, MSAVI, NDGI, NDVI, SAVI, and TVI (Figure 11). In the raining season, only the slope-based VIs, namely: NDVI, TVI, NDGI, GNDVI, and ARVI with the exception of EVI, displayed a negative correlation with the LST

(Figure 12). This means EVI is the only slope-based VIs that demonstrated a positive correlation with the LST in raining season. However, in the raining season, LST had a positive linear correlation with the three distance-based VIs: DVI, SAVI, and MSAVI. Negative correlations between LST and VIs suggested that an increase in the LST corresponded to a drop in VI values during the dry season. Similarly, positive correlations between LST and VIs indicated that an increase in LST corresponded to an increase in VI values during the dry season. It is worth noting that the positive correlation between the LST and the distance-based VIs: SAVI, MSAVI, and DVI during the rainy season can be attributed to the fact that they compensate for a mix of green vegetation and soil background.

The relationship between LST and VIs can also be interpreted by Preveldello et al. (2019), who explained that vegetation generally has low albedo (i.e. low surface reflectance) due to cragginess of the leaves, which leads to high heat absorption; compared to high albedo (high surface reflectance) due to smoothness of the surface, which leads to lower heat absorption. Therefore, negative NDVI values, for example, indicate a body of water, whereas low NDVI values (between 0 and 0.1) suggest barren soil and values over 0.25 indicate vegetation. From the foregoing, high LST corresponded to bare soil (due to high albedo, i.e. lesser heat absorption) and low LST corresponded to vegetated area (due to low surface reflectance) in the dry season.

The finding of a negative correlation between LST and NDVI in the dry and rainy seasons is consistent with the findings of Sun & Kafatos (2007), Liang et al. (2012), Ghobadi et al. (2015), Al-Khudhairy & Al-Timimi (2021) and Guechi et al. (2021), who revealed a negative correlation between LST and NDVI. Furthermore, the negative correlation between LST and SAVI in the dry season was consistent with the findings of Guechi et al. (2021). In addition, the negative correlation between LST and NDVI and EVI agrees with the findings by Alademomi et al. (2020).

Table 5. Linear regression between LST and VIs

S/N	Dry Season			Rainy Season		
	Linear Regression	r		Linear Regression	r	
1	LST = -5.537 NDVI + 35.43	0.638	-	LST = -0.577 NDVI + 29.777	0.075	-
2	LST = -15.282 DVI + 34.178	0.375	-	LST = 3.616 DVI + 28.824	0.134	+
3	LST = -10.709 EVI + 34.738	0.489	-	LST = 0.788 EVI + 29.126	0.053	+
4	LST = -10.819 TVI + 43.459	0.639	-	LST = -2.423 TVI + 32.027	0.106	-
5	LST = -6.815 NDGI + 31.603	0.359	-	LST = -3.152 NDGI + 29.215	0.245	-
6	LST = -9.221 GNDVI + 38.325	0.664	-	LST = -0.031 GNDVI + 29.39	0.003	-
7	LST = -4.083 ARVI + 34.08	0.598	-	LST = -1.262 ARVI + 30.167	0.197	-
8	LST = -10.411 SAVI + 34.841	0.485	-	LST = 1.787 SAVI + 28.806	0.112	+
9	LST = -10.502 MSAVI + 34.505	0.445	-	LST = 2.072 MSAVI + 28.794	0.136	+

NOTE: Generated at Confidence Interval of 99% (p-values < 0.01). r = coefficient of correlation.
Positive values = positive correlation and negative values = negative correlation. Sample points = 668.

In terms of the strength of the connection between the LST and the VIs in the dry season (as shown in Table 5), the correlations between the LST and the VIs were all statistically and highly significant (p-values 0.01). GNDVI performed best with a normal correlation coefficient (r=0.664), followed by TVI (r=0.639), NDVI (r=0.638), and ARVI (r=0.598). This findings implied that there was a significant amount of LST in the study area during dry season. The findings are supported by the fact that the data was collected during the scorching month of March. Furthermore, EVI performed less having a weak correlation coefficient of 0.489, followed by SAVI (0.485), MSAVI (0.445), TVI (r=0.375), and NDGI (r=0.359) respectively.

Consequently, in terms of the strength of the correlation of the LST versus the VIs during the rainy season, all of the VIs performed very weakly against the LST. Their performance is listed in descending order as follows: ARVI (r=0.197) > MSAVI (r=0.136) > DVI (r=0.134) > SAVI (r=0.112) > TVI (r=0.106) > NDVI (r=0.075) > EVI (0.053) > GNDVI (r=0.245) (0.003). The findings indicated that the LST in the studied region was low during the rainy season. This conclusion can be pinned to the fact that the rainy season data was taken in August, when rainfall

is often at its peak. The study revealed that the correlations between LST and NDVI, as well as other VIs, vary depending on the season.

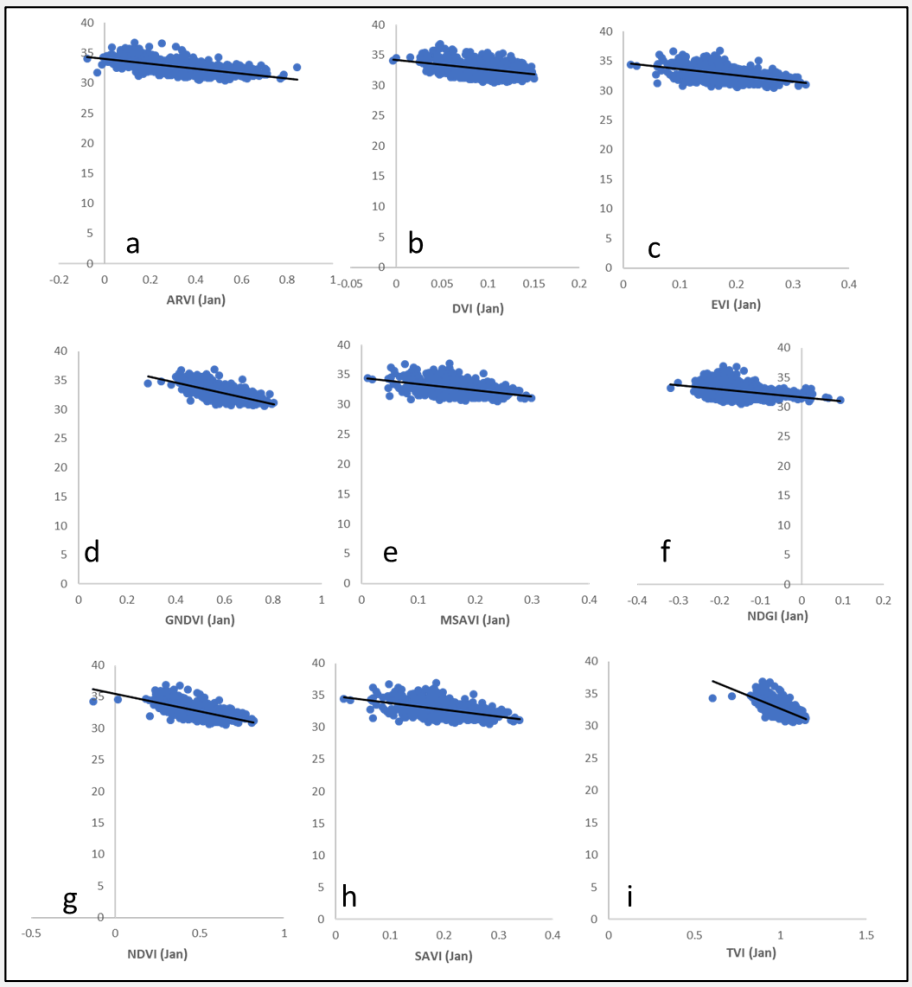

Figure 11. Scatterplots of LST versus VIs for dry season. (a) ARVI; (b) DVI; (c) EVI; (d) GNDVI; (e) MSAVI; (f) NDGI; (g) NDVI; (h) SAVI; (i) TVI.

However, Sun & Kafatos (2007) found a positive correlation between the NDVI and the LST in winter, and only during the warm seasons were there high negative correlations between LST and NDVI. Karnieli et al. (2006) found that positive correlations between LST and NDVI existed at the northern ecosystems at high latitudes. As a result, LST-VI feature space might change greatly depending on the season and underlying surface type. It means, each ecosystem has its own set of variable atmospheric conditions. Importantly, because a high LST corresponds to a low NDVI and vice versa, the negative correlation between LST-NDVI is relevant for urban climate research and other fields of science (Carlson et al., 1994; Anbazhagan et al., 2016, Macarof et al., 2018). The Vis other than the NDVI that have a negative correlation with LST can also be employed for climate-related research.

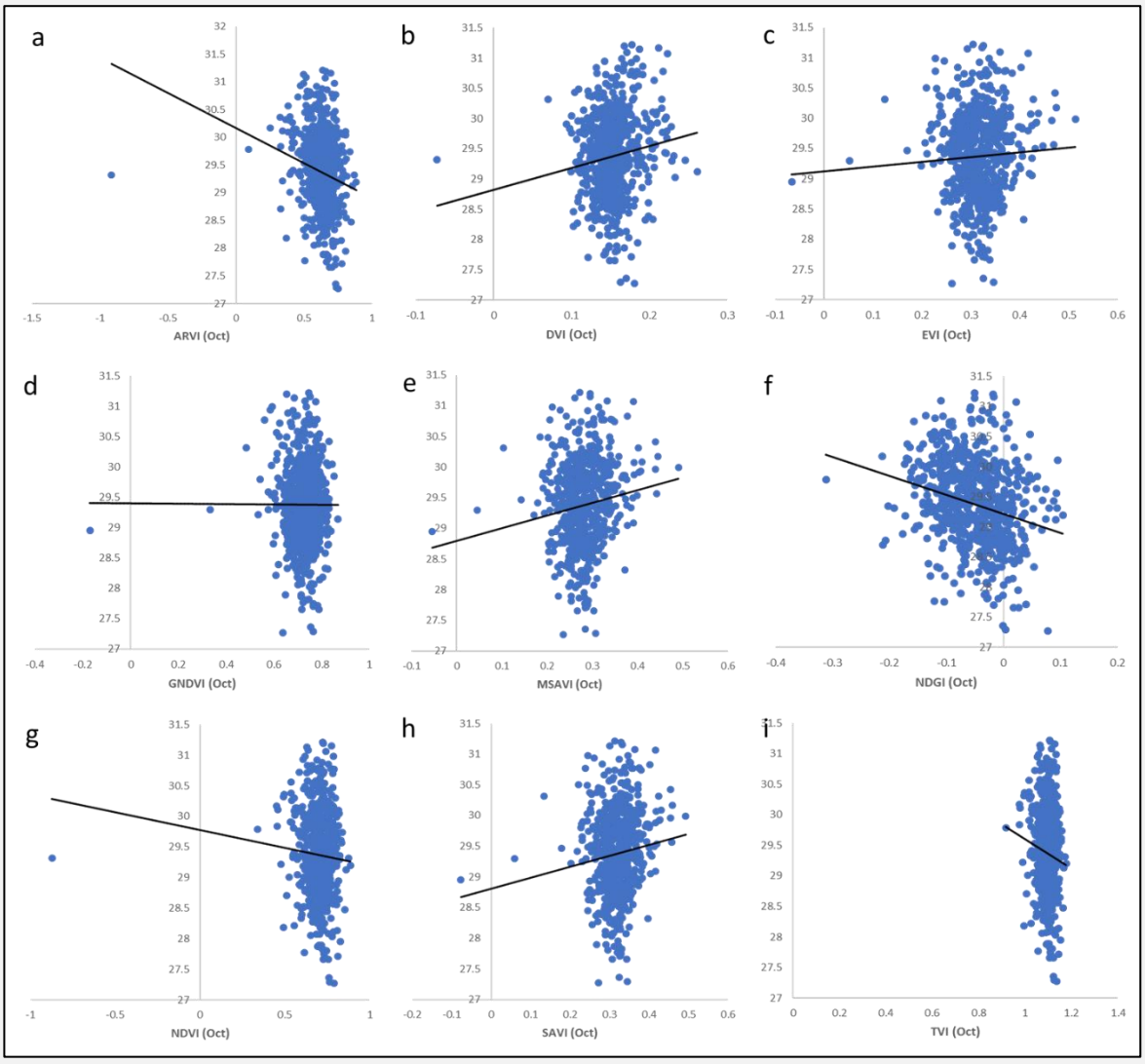

Figure 11. Scatterplots of LST versus VIs for rainy season. (a) ARVI; (b) DVI; (c) EVI; (d) GNDVI; (e) MSAVI; (f) NDGI; (g) NDVI; (h) SAVI; (i) TVI.

CONCLUSION

The current study used regression analysis and GIS to examine the seasonal correlation between spectral vegetation indices against the LST and NDVI in dry and raining season. The study of the forest area revealed some similarities and differences in the NDVI-VIs and LST-NDVI relationships. The study concluded that based on the coefficient of variation, the VIs displayed homogeneity in their spread or dispersion across the study area during both the dry and raining seasons. In both dry and rainy seasons, all VIs demonstrated a positive linear correlation with the NDVI. The underlying reason for the trend of the VIs versus the NDVI can be attributed to the fact that the mathematical expression of the VIs comprises either an NIR or a red band, which is shared by all VIs. Importantly, visual inspection of the derived Vis indicated that the ARVI, GNDVI, and TVI showed a resemblance with the NDVI. This was further corroborated by the regression analysis in which the ARVI, GNDVI and TVI had a strong correlation with the NDVI in both dry and raining seasons. It can be concluded that the ARVI, GNDVI and TVI performed well with NDVI and can be used to supplant NDVI for vegetation related studies in the study area. The three (3) distance-based VIs, namely DVI, SAVI, and MSAVI showed a normal correlation with the NDVI throughout both the dry and rainy seasons, with the exception of the SAVI, which had a strong correlation with the NDVI during the rainy season. For the LST-Vis relationship, the GNDVI, TVI, NDVI, and

ARVI had a normal correlation coefficient with the LST in the dry season. This result further corroborates the performance of the ARVI, GNDVI, and TVI against the NDVI to be the appropriate VIs for the study area. The study further concluded that the feature space of the LST versus the ARVI, GNDVI, NDVI, and TVI can be used for climate related studies such as plant health, soil heat content, drought damage, anomalous heat fluctuation due to urbanization, and other surface material properties in the study area. For the raining season, the LST had a weak negative correlation with the slope-based VI (NDVI, ARVI, GNDVI, TVI, EVI, NDGI), while it surprisingly had a weak positive correlation with the distance-based VIs (DVI, SAVI, and MSAVI). The current study advances the knowledge on the performance of some slope-based and distance-based VIs versus the NDVI and LST in the study area. It is however suggested that the study should be conducted in other forest or similar areas to confirm this trend.

ACKNOWLEDGEMENTS

The authors would like to acknowledge the U. S. Geological Survey and the National Aeronautics and Space Administration (NASA) for the provision of the Landsat imagery and MODIS datasets for this study. The authors also thank the anonymous reviewers for their observations/contributions to the study.

REFERENCES

AlAdemomi, A. S., Okolie, C. J., Daramola, O. E., Agboola, R. O., & Salami, T. J. (2020). Assessing the relationship of LST, NDVI and EVI with land cover changes in the Lagos Lagoon environment. *Quaestiones Geographicae*, *39*(3), 87-109. https://doi.org/10.2478/quageo-2020-0025

Al-Khudhairy, A. A., & Al-Timimi, Y. K. (2021). Analysis of the LST and Vegetation Indices relationship using Landsat-8 data in Duhok Governorate, Iraq. *Al-Mustansiriyah Journal of Science, 32*(4), 6-12.

Amidon, W. (2014). *Dark object subtraction in ENVI.* [Video file). Retrieved from: https://www.youtube.com/watch?v=QYrgIRO6JiY.

Anbazhagan, S., & Paramasivam, C. R. (2016). Statistical correlation between land surface temperature (LST) and vegetation index (NDVI) using multi-temporal landsat TM data. *International Journal of Advanced Earth Science and Engineering*, *5*(1), 333-346.

Baig, M. H. A., Zhang, L., Shuai, T., & Tong, Q. (2014). Derivation of a tasselled cap transformation based on Landsat 8 at-satellite reflectance. *Remote Sensing Letters*, *5*(5), 423-431. https://doi.org/10.1080/2150704X.2014.915434

Baret, F., & Guyot, G. (1991). Potentials and limits of vegetation indices for LAI and APAR assessment. *Remote sensing of environment*, *35*(2-3), 161-173. https://doi.org/10.1016/0034-4257(91)90009-U

Carlson, B. E., Lacis, A. A., & Rossow, W. B. (1994). Belt-zone variations in the Jovian cloud structure. *Journal of Geophysical Research: Planets*, *99*(E7), 14623-14658. https://doi.org/10.1029/94JE01222

Carlson, T. N., & Ripley, D. A. (1997). On the relation between NDVI, fractional vegetation cover, and leaf area index. Remote sensing of Environment, 62(3), 241-252. https://doi.org/10.1016/S0034-4257(97)00104-1

Chandra, P. (2011). Performance evaluation of vegetation indices using remotely sensed data. *International Journal of Geomatics and Geosciences*, *2*(1), 231-240.

Chavez Jr, P. S. (1988). An improved dark-object subtraction technique for atmospheric scattering correction of multispectral data. *Remote sensing of environment*, *24*(3), 459-479. https://doi.org/10.1016/0034-4257(88)90019-3

Chu, D. (2019). *Remote sensing of land use and land cover in mountain region: a comprehensive study at the central Tibetan Plateau*. Springer Singapore.

Cohen, J., Cohen, P., West, S. G. & Aiken, L. S. (2002). *Applied multiple regression/correlation analysis for the behavioral sciences (3rd ed.)*. Routledge, New York: 536. https://doi.org/10.4324/9780203774441

Deering, D. W., Rouse, J. W., Haas, R. H. & Schell, J. A. (1975). Measuring forage production of grazing units from Landsat MSS data. *Proceeding of the 10th International Symposium on Remote Sensing of Environment*. II: 1169-1178.

Deng, Y., Wang, S., Bai, X., Tian, Y., Wu, L., Xiao, J., Chen, F., & Qian, Q. (2018). Relationship among land surface temperature and LUCC, NDVI in typical karst area. *Scientific reports*, *8*(1), 1-12. https://doi.org/10.1038/s41598-017-19088-x

Falk, M., Meyers, T., Black, A., Barr, A., Yamamoto, S., Verma, S., Heinsch, F. A. & Baldocchi, D. (2004). On handshaking vegetation indices from tower to MODIS pixel scale: comparing broadband ndvi tower measurements with satellite data products, *MODIS Vegetation Workshop II*, Missoula, Montana.

Gao, X., Huete, A. R., Ni, W., & Miura, T. (2000). Optical–biophysical relationships of vegetation spectra without background contamination. *Remote sensing of environment*, *74*(3), 609-620. https://doi.org/10.1016/S0034-4257(00)00150-4

Geospatial Science (GSP). (2019). *GSP 216: Introduction to remote sensing: radiometric calibration and corrections*. [Lecture Note – Humboldt State University]. https://gsp.humboldt.edu/OLM/Courses/GSP_216_Online/lesson4-1/radiometric.html

Ghobadi, Y., Pradhan, B., Shafri, H. Z. M., & Kabiri, K. (2015). Assessment of spatial relationship between land surface temperature and landuse/cover retrieval from multi-temporal remote sensing data in South Karkheh Sub-basin, Iran. *Arabian Journal of Geosciences*, *8*(1), 525-537. https://doi.org/10.1007/s12517-013-1244-3

Gilmore, S., Saleem, A. & Dewan, A. (2015). *Effectiveness of DOS (dark-object subtraction) method and water index techniques to map wetlands in a rapidly urbanizing megacity with Landsat 8 data*. In: *Research@Locate'15*. Brisbane; 10-12. http://hdl.handle.net/20.500.11937/43918

Gitelson, A. A., Kaufman, Y. J., & Merzlyak, M. N. (1996). Use of a green channel in remote sensing of global vegetation from EOS-MODIS. *Remote sensing of Environment*, *58*(3), 289-298. https://doi.org/10.1016/S0034-4257(96)00072-7

Gitelson, A., Zur, Y., Chivkunova, O. B., & Merzlyak, M. N. (2002). Assessing carotenoid content in plant leaves with reflectance spectroscopy. *Photochemistry and Photobiology*, *75*(3), 272-281. https://doi.org/10.1562/0031-8655(2002)0750272ACCIPL2.0.CO2

Guechi, I., Gherraz, H., & Alkama, D. (2021). Correlation analysis between biophysical indices and Land Surface Temperature using Remote Sensing and GIS in Guelma City (Algeria). *Bulletin de la Société Royale des Sciences de Liège*, *90*, 158-180. https://doi.org/10.25518/0037-9565.10457

Guha, S., Govil, H., & Diwan, P. (2020). Monitoring LST-NDVI relationship using premonsoon Landsat datasets. *Advances in Meteorology*, 1-15. https://doi.org/10.1155/2020/4539684

Haboudane, D., Miller, J. R., Pattey, E., Zarco-Tejada, P. J., & Strachan, I. B. (2004). Hyperspectral vegetation indices and novel algorithms for predicting green LAI of crop canopies: modeling and validation in the context of precision agriculture. *Remote Sensing of Environment, 90(3)*, 337-352. https://doi.org/10.1016/j.rse.2003.12.013

Hao, X., Li, W., & Deng, H. (2016). The Oasis Effect and Summer Temperature Rise in Arid Regions-Case Study in Tarim Basin. *Scientific Reports, 6*, 35418. https://doi.org/10.1038/srep35418

Higginbottom, T. P., & Symeonakis, E. (2014). Assessing land degradation and desertification using vegetation index data: current frameworks and future directions. *Remote Sensing, 6*, 9552-9575. https://doi.org/10.3390/rs6109552

Holme, S., Heaton, W. A., & Courtright, M. (1987). Improved in vivo and in vitro viability of platelet concentrates stored for seven days in a platelet additive solution. *British journal of haematology*, *66*(2), 233-238. https://doi.org/10.1111/j.1365-2141.1987.tb01304.x

Huete, A. R. (1988). A soil-adjusted vegetation index (SAVI). *Remote Sensing of Environment, 25*(3), 295-309.

Huete, A. R., Liu, H. Q., Batchily, K. V., & Van Leeuwen, W. J. D. A. (1997). A comparison of vegetation indices over a global set of TM images for EOS-MODIS. *Remote sensing of environment*, *59*(3), 440-451. https://doi.org/10.1016/S0034-4257(96)00112-5

Huete, A., Didan, K., Miura, T., Rodriguez, E. P., Gao, X., & Ferreira, L. G. (2002). Overview of the radiometric and biophysical performance of the MODIS vegetation indices. *Remote sensing of environment*, *83*(1-2), 195-213. https://doi.org/10.1016/S0034-4257(02)00096-2

Jensen, J. (2007). *Remote sensing of the environment*. Pearson Prentice Hall.

Kafer, P. S., Rocha, N. S., Diaz, L. R., Kaiser, E. A., Costa, S. T. L., Hallal, G., Veeck, G., Roberti, D., & Rolim, S. B. A. (2020). Seasonal assessment of surface temperature with normalized vegetation index and surface albedo over Pampa biome. *The International Archives of the Photogrammetry, Remote Sensing and Spatial Information Sciences, XLII-3/W12*. https://doi.org/10.1109/LAGIRS48042.2020.9165660

Kamuku National Park. (2022). Retrieved from: https://placeandsee.com/wiki/kamuku-national-park. Accessed on: 7 July, 2022.

Karnieli, A., Bayasgalan, M., Bayasgalan, Y., Agam, N., Khudulmur, S., & Tucker, C. J. (2006). Comments on the use of the vegetation health index over Mongolia. International Journal of Remote Sensing, 27(10), 2017-2024. https://doi.org/10.1080/01431160500121727

Kaufman, Y. J., & Tanre, D. (1992). Atmospherically resistant vegetation index (ARVI) for EOS-MODIS. *IEEE transactions on Geoscience and Remote Sensing*, *30*(2), 261-270. https://doi.org/10.1109/36.134076

Khandelwal, S., Goyal, R., Kaul, N., & Mathew, A. (2018). Assessment of land surface temperature variation due to change in elevation of area surrounding Jaipur, India. *The Egyptian Journal of Remote Sensing and Space Science*, *21*(1), 87-94. https://doi.org/10.1016/j.ejrs.2017.01.005

Koko, A. F., Yue, W., Abubakar, G. A., Alabsi, A. A. N., & Hamed, R. (2021). Spatiotemporal influence of land use/land cover change dynamics on surface urban heat island: A case study of Abuja metropolis, Nigeria. *ISPRS International Journal of Geo-Information, 10*(3), 248. https://doi.org/10.3390/ijgi10050272

Land Processes Distribution Active Archive Data, LP DAAC, (2017). Getting started with MODIS land surface temperature data (Part 2) [Video file]. Retrieved from: https://www.youtube.com/watch?v=w_Y41y4UogQ.

Lawrence, R. L., & Ripple, W. J. (1998). Comparisons among vegetation indices and bandwise regression in a highly disturbed, heterogeneous landscape: Mount St. Helens, Washington. *Remote Sensing of environment*, *64*(1), 91-102. https://doi.org/10.1016/S0034-4257(97)00171-5

Liang, B. P., Li, Y. & Chen, K. Z. A (2012). Research on Land Features and Correlation between NDVI and Land Surface Temperature in Guilin City. *Remote Sensing Technology and Application, 27*(3), 429–435.

Liang, S. (2005). *Quantitative Remote Sensing of Land Surfaces*. John Wiley and Sons.

Lopresti, M. F., Di Bella, C. M., & Degioanni, A. J. (2015). Relationship between MODIS-NDVI data and wheat yield: A case study in Northern Buenos Aires province, Argentina. *Information Processing in Agriculture*, *2*(2), 73-84. https://doi.org/10.1016/j.inpa.2015.06.001

Maas, S. J., & Rajan, N. (2010). Normalizing and converting image dc data using scatter plot matching. *Remote Sensing, 2*(7), 1644–1661. https://doi.org/10.3390/rs2071644

Macarof, P. Groza, S. & Statescu, F. (2018). Investigating correlation lst and vegetation indices using landsat images for the warmest month: a case study of Lasi County. Annals of Valahia University of Targoviste. Geographical Series, 18(1), 33-40. https://10.2478/avutgs-2018-0004

Moulin, S. (1999). Impacts of model parameter uncertainties on crop reflectance estimates: a regional case study on wheat. *International Journal of Remote Sensing*, *20*(1), 213-218. https://doi.org/10.1080/014311699213730

Njomo, D. (2008). Mapping deforestation in the Congo basin forest using multi-temporal spot-vgt imagery from 2000 to 2004. *EARSeLs eProceedings, 7*(1), 1. Retrieved from https://www.researchgate.net/publication/252273821. Accessed on April 25, 2022.

O'neil-Dunne, J. (2014). *Dark object subtraction* [Video file]. Retrieved from https://www.youtube.com/watch?v=uXLzeTJG_to.

Panda, S. S., Ames, D. P., & Panigrahi, S. (2010). Application of vegetation indices for agricultural crop yield prediction using neural network techniques. *Remote Sensing, 2*(3), 673-696. https://doi.org/10.3390/rs2030673

Panek, E., Gozdowski, D., Stepien, M., Samborski, S., Rucinski, D., & Buszke, B. (2020). Within-field relationships between satellite-derived vegetation indices, grain yield, and spike number of winter wheat and triticale. *Agronomy, 10*(11), 1842. https://doi.org/10.3390/agronomy10111842

Pinty, B., & Verstraete, M. M. (1992). GEMI: a non-linear index to monitor global vegetation from satellites. *Vegetatio*, *101*(1), 15-20. https://doi.org/10.1007/BF00031911

Purkis, S. J., & Klemas, V. V. (2011). *Remote sensing and global environmental change*. John Wiley and Sons.

Qi, J., Chehbouni, A., Huete, A. R., Kerr, Y. H., & Sorooshian, S. (1994). A modified soil adjusted vegetation index. *Remote Sensing of Environment*, *48*(2), 119–126. https://doi.org/10.1016/0034-4257(94)90134-1

Rouse, J. (1974). *Monitoring the vernal advancement and retrogradation (green wave effect) of natural vegetation*. NASA Technical Reports Server. Retrieved from https://ntrs.nasa.gov/search.jsp?R=19740022555

Rouse, J. W. (1973). Monitoring vegetation systems in the Great Plains with ERTS-1. In *3rd Earth Resources Technology Satellite Symposium, 1973*.

Salas, E. A. L., & Henebry, G. M. (2014). A new approach for the analysis of hyperspectral data: theory and sensitivity analysis of the moment distance method. *Remote Sensing*, *6*(1), 20-41. https://doi.org/10.3390/rs6010020

She, X., Zhang, L., Cen, Y., Wu, T., & Huang, C. (2015). Comparison of the continuity of vegetation indices derived from Landsat 8 OLI and Landsat 7 ETM+ Data among Different Vegetation Types. *Remote Sensing*, *7*(10), 13485-13506. https://doi.org/10.3390/rs71013485

Silleos, N. G., Alexandridis, T. K., Gitas, I. Z., & Perakis, K. (2006). Vegetation indices: advances made in biomass estimation and vegetation monitoring in the last 30 years. *Geocarto International*, *21*(4), 21-28. https://doi.org/10.1080/10106040608542399

Sun, D., & Kafatos, M. (2007). Note on the NDVI-LST relationship and the use of temperature-related drought indices over North America. *Geophysical Research Letters, 34*(24), L24406. https://doi.org/10.1029/2007GL031485

Tariq, A., Riaz, I., Ahmad, Z., Yang, B., Amin, M., Kausar, R., Andleeb, S., Farooqi, M. A., & Muhammad, R. (2020). Land surface temperature relation with normalized satellite indices for the estimation of spatio-temporal trends in temperature among various land use land cover classes of an arid Potohar region using Landsat data. *Environmental Earth Sciences, 79*(1), 40. https://doi.org/10.1007/s12665-019-8766-2

Tomlinson, C. J., Chapman, L., Thornes, J. E., & Baker, C. (2011). Remote sensing land surface temperature for meteorology and climatology: A review. *Meteorological Applications*, *18*(3), 296-306. https://doi.org/10.1002/met.287

Tucker, C. J. (1979). Red and photographic infrared linear combinations for monitoring vegetation. *Remote sensing of Environment*, *8*(2), 127-150. https://doi.org/10.1016/0034-4257(79)90013-0

UNESCO (2022). *Kwiambana and/or Ningi: description*. Retrieved from https://whc.unesco.org/en/tentativelists/492/. Accessed on: 7 July, 2022.

Vogelmann, J. E. (1990). Comparison between two vegetation indices for measuring different types of forest damage in the north-eastern United States. *International Journal of Remote Sensing, 11*(12), 2281-2297. https://doi.org/10.1080/01431169008955175

Wan, Z. (2013). *MODIS land surface temperature products: Users' Guide*. Retrieved from https://icess.eri.ucsb.edu/modis/LstUsrGuide/usrguide.html.

Wang, F., Huang, J., & Chen, L. (2015). Development of a vegetation index for estimation of leaf area index based on simulation modeling. Journal of Plant Nutrition, 33(3), 328–338. https://doi.org/10.1080/01904160903470380.

Wang, Z., Lu, Z., & Cui, G. (2020). Spatiotemporal variation of land surface temperature and vegetation in response to climate change based on NOAA-AVHRR data over China. *Sustainability, 12*(9), 3601. https://doi.org/10.3390/su12093601

Xiong, Y. J., & Qiu, G. Y. (2011). Estimation of evapotranspiration using remotely sensed land surface temperature and the revised three-temperature model. *International Journal of Remote Sensing, 32*(20), 5853-5874. https://doi.org/10.1080/01431161.2010.507791

Xu, D., Kang, X., Qiu, D., Zhuang, D., & Pan, J. (2009). Quantitative assessment of desertification using landsat data on a regional scale – a case study in the Ordos Plateau, China. *Sensors, 9*(3), 1738-1753. https://doi.org/10.3390/s90301738

Yale (2013). *Converting digital numbers to top of atmosphere (TOA) reflectance*. The Yale Center for Earth Observation, Yale University. Retrieved from: http://www.yale.edu/ceo.

Yengoh, G. T., Dent, D., Olsson, L., Tengberg, A. E., & Tucker III, C. J. (2015). *Use of the Normalized Difference Vegetation Index (NDVI) to assess Land degradation at multiple scales: current status, future trends, and practical considerations*. Springer.

Yuan, X. L., Wang, W., Cui, J., Meng, F., Kurban, A., & Maeyer, P. (2017). Vegetation changes and land surface feedbacks drive shifts in local temperatures over Central Asia. Scientific Reports, 7, 3287. https://doi.org/10.1038/s41598-017-03432-2

Zhang, C., & Kovacs, J. M. (2012). The application of small unmanned aerial systems for precision agriculture: A review. *Precision Agriculture, 13*(6), 693–712. https://doi.org/10.1007/s11119-012-9274-5

Zhang, X., Wu, S., Yan, X., & Chen, Z. (2016). A global classification of vegetation based on NDVI, rainfall, and temperature. International Journal of Climatology, 37. doi:10.1002/joc.4847

Zhang, X., Wu, S., Yan, X., & Chen, Z. (2017). A global classification of vegetation based on NDVI, rainfall and temperature. *International Journal of Climatology*, *37*(5), 2318-2324. https://doi.org/10.1002/joc.4847

Zhou, Y., Zhang, L., Xiao, J., Chen, S., Kato, T., Zhou, G., Zhou, Y., Zhang, L., Xiao, J., Chen, S., Kato, T., & Zhou, G. (2014). A comparison of satellite-derived vegetation indices for approximating gross primary productivity of grasslands. *Rangeland Ecology & Management, 67*(1), 9–18. https://doi.org/10.2111/REM-D-13-00059.1